Structure
Ways & Means

Improving Structure-Based Function Prediction Using Molecular Dynamics

Dariya S. Glazer,[1] Randall J. Radmer,[2] and Russ B. Altman[1,2,3,*]
[1]Department of Genetics
[2]SIMBIOS National Center
[3]Department of Bioengineering
Stanford University, 318 Campus Drive, Clark Center, Stanford, CA 94305, USA
*Correspondence: russ.altman@stanford.edu
DOI 10.1016/j.str.2009.05.010

SUMMARY

The number of molecules with solved three-dimensional structure but unknown function is increasing rapidly. Particularly problematic are novel folds with little detectable similarity to molecules of known function. Experimental assays can determine the functions of such molecules, but are time-consuming and expensive. Computational approaches can identify potential functional sites; however, these approaches generally rely on single static structures and do not use information about dynamics. In fact, structural dynamics can enhance function prediction: we coupled molecular dynamics simulations with structure-based function prediction algorithms that identify Ca^{2+} binding sites. When applied to 11 challenging proteins, both methods showed substantial improvement in performance, revealing 22 more sites in one case and 12 more in the other, with a modest increase in apparent false positives. Thus, we show that treating molecules as dynamic entities improves the performance of structure-based function prediction methods.

INTRODUCTION

Understanding the function of molecules is the first step toward learning how to manipulate them. Experimental techniques for determining molecular function tend to be expensive and time-consuming. Consequently, computational methods can be critical for establishing molecular function. Some techniques use similarity in the sequence of molecules: when protein sequences are at least 40% similar, they usually perform similar functions and so annotations can be transferred with some confidence. However, when sequence similarity falls below 40%, the reliability of these methods decreases (Wilson et al., 2000).

Some molecular sites of interest, such as binding pockets and enzyme active sites, might not be recognized with sequence patterns alone, because they might be comprised of loop segments that come together in three dimensions, but are distant in the primary sequences. In these cases, similarity might exist on the structural level even when there is no detectable similarity in the corresponding sequences. In order to address this challenge, many structure-based function recognition methods use shared 3D structural environments or "3D motifs" to recognize molecular functions (Fetrow et al., 1998; Halperin et al., 2008; Wallace et al., 1997). Some methods also combine information from sequence and structure (Friedberg, 2006; Watson et al., 2005).

Since the initiation of the structural genomics (SG) efforts, the number of solved structures in the Protein Data Bank (PDB) (Berman et al., 2000) with unknown function is increasing (Chandonia and Brenner, 2006; Levitt, 2007; Terwilliger, 2004). SG efforts specifically target proteins with little sequence similarity to functionally annotated folds. Therefore, structure-based function annotation methods able to recognize distant functional relationships would be very useful (Halperin et al., 2008; Nayal and Di Cera, 1994).

The structures from the X-ray crystallographic studies in the PDB typically provide static snapshots of molecules that are averages of the structures in the crystal lattice. Crystal packing induced by crystallization conditions and experimental modifications required to facilitate experimental studies might create slight variations of the structures that do not represent the biologically functional conformations. This might frustrate attempts to annotate function based on detailed analysis of the structures.

While performing their functions, molecules undergo dynamic structural changes, which can range from subtle side-chain rearrangements to large-scale domain movements (Henzler-Wildman and Kern, 2007). Physics-based molecular dynamics (MD) simulations allow structural investigation of such motions on the femtosecond, nanosecond, and occasionally microsecond scales (Karplus and Kuriyan, 2005; Karplus and McCammon, 2002). These motions might reveal conformations relevant to molecular functions. At the very least, sampling near the crystal structure might help in identifying structural motifs that are not obvious in a single static structure.

The idea of using information about dynamics to improve functional analysis is not new. Alternative X-ray structures, nuclear magnetic resonance ensembles, and MD-generated trajectories all provide information about dynamics useful for structure-based drug design (Damm and Carlson, 2007; Huang and Zou, 2007; Meagher and Carlson, 2004; Sivanesan et al., 2005; Wong et al., 2005). Eyrisch and coworkers (Eyrisch and Helms, 2007) used an algorithm to locate surface pockets in structures generated by the MD simulations, where those were not apparent in the original crystal structures. Among those transient surface pockets were the actual active sites of the molecules. Frembgen-Kesner and Elcock (2006) also demonstrated that

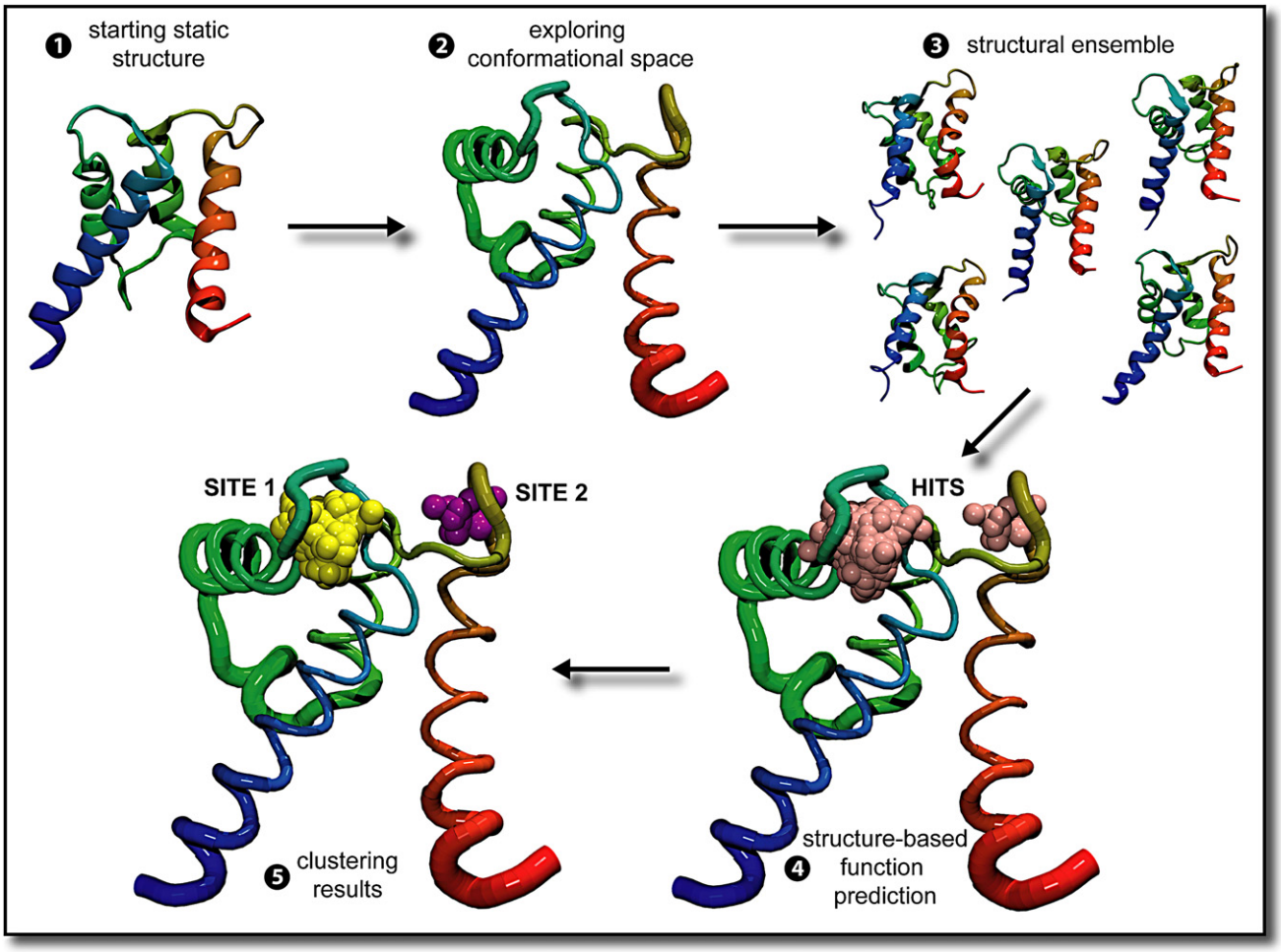

Figure 1. Overview of the Scheme

(1 and 2) A structure from the PDB is chosen and simulated using molecular dynamics. In our case, 11 HOLO and corresponding 11 APO structures were obtained and simulation trajectory was generated for 1 ns.

(3) A structural ensemble is formed with frames extracted from the simulation trajectory, in our case every 2.5 picoseconds.

(4) A structure-based function prediction method, such as FEATURE or the valence method, is used to examine the structural ensemble.

(5) A clustering scheme defines how many sites the structure-based function prediction methods identified, and might also assign which of those are true positive. In 2, 4, and 5, the thickness of the ribbon representing the backbone of the molecule represents how much of the conformational space that part of the molecule sampled over the course of the simulation. As such, in this molecule the termini and the flexible loops are thicker, because they moved more, whereas the α helices are thinner, especially where the three of them form a sheet, because they did not move much.

coupling a docking method with MD simulations uncovers cryptic drug binding sites.

In this article, we describe our work in improving the performance of structure-based function recognition methods by coupling them to molecular dynamics (see Figure 1). The MD simulations demonstrated formation of favorable, albeit transient, conformations that suggest functions not apparent in the initial PDB structures. Specifically, for 11 different molecules we used FEATURE (Wei and Altman, 2003) and a valence-based method (Nayal and Di Cera, 1994) to analyze the presence of Ca^{2+} binding sites in 22 structural ensembles generated by the MD simulations using GROMACS.

Calcium plays a crucial role within many signaling pathways in the cell. Recognizing the ability of molecules to bind calcium might permit manipulations with direct impact on many aspects of cell life. Ca^{2+} binding sites tend to occur within flexible loops of the molecules and be oxygen rich, with several glutamate and aspartate residues lining the pocket. Often solvent molecules are also involved, because the binding occurs at the surface of the molecule. The straightforward coordination of calcium binding sites makes it surprising that the leading function-recognition methods fail to identify them even within structures with bound calcium. We show that allowing function recognition methods to examine the dynamic nature of the molecules dramatically improves their performance.

RESULTS

The 11 molecules studied here have at least one documented calcium-binding site (see Table 1 and Discussion). For each of

Table 1. Final Results of FEATURE ± MD and Valence ± MD Scanning

PDB ID	Size (# AA)	RMSD (Å)	Exp #	Feature (50)		Valence (1.4)	
				−MD	+MD	−MD	+MD
1B9A	108	1.423	2	2	2	0	2
1B8C			1	1	1	0	0
1K94	217	1.234	2	1	1 [1]	0	2
1F4Q			2	1	1 [1]	0	0
3DNI	260	1.750▲	3	1	3	1	2
1DNK			3	1	2	0	0
1I40	175	0.625	3	1	2 *	0	1
1MJW			3	0	0	0	0
1K96	90	4.067	2	2	2	1	2
1K8U			2	0	0	0	0
1PSH	119	0.613	1	0	0 [1]	0	0
1A3D			1	0	1	0	0
1NLS	237	0.371	1	1	1 [1]	0	1
1DQ0			1	0	1	0	0
1F6S	123	1.194▲	1	0	1 [1]	0	1
1F6R			1	1	1 [1]	0	0
3LHM	130	0.211	1	0	1 [1]	1	1
2LHM			1	0	1 [1]	0	0
1QMD	370	0.203	4	0	4 [1] *	0	2
1QM6			4	0	4 [4] *	0	0
2POR	301	0.939	4	1	4 [1]	0	1
3POR			4	2	4 [2]	0	0
Total H			24	9	21 [7]	3	15
Total A			23	6	16 [9]	0	0
Total			47	15	37 [16]	3	15

The first column lists PDB IDs of the structures used in this work. The eleven molecules are listed in order, with HOLO structure (e.g., 1B9A) being followed by the corresponding APO structure (e.g., 1B8C) for each protein. The number of amino acids comprising each molecule is listed in column two. The next column lists the backbone RMS deviation between the HOLO and the APO structures used to start MD simulations for each molecule. The symbol ▲ denotes that the original PDB file of at least one of the structures in the pair has missing atoms or residues (see Supplemental Experimental Procedures section 1). The fourth column reports how many true Ca^{2+} binding sites there are in each structure. The next two columns report the global FEATURE scanning results for analysis of initial PDB structures and structural ensembles. The last two columns report the global valence-based method results for the starting PDB structures and structural ensembles. Superscript numbers inform how many false positive results were obtained. See the Results section for explanations of the results marked by *.

the molecules at least two structures exist in the PDB: a HOLO form, with Ca^{2+} bound within the structure, and an APO one, without a bound Ca^{2+}. Existing methods for structure-based function recognition often do not identify the APO sites, and even can miss the HOLO sites. As such, these structures make an excellent set of test cases. In addition to revealing the concealed Ca^{2+} binding sites in the HOLO structures, can simulation identify the binding sites in the APO structures?

Preparation of Structures

In 5 of the 11 pairs of structures the two partners do not have identical sequences, because one contains at least one mutation. In four pairs these mutations are far from the Ca^{2+} binding sites. In one HOLO – APO pair, namely 1B9A-1B8C, a mutation affecting residue 101 (GLU to ASP) appears in the coordinating loop of the 1B8C CA109 site. This mutation in the APO modifies the affinity of Ca^{2+} binding at the CA109 site and eliminates Ca^{2+} binding at the CA110 site (Cates et al., 1999). As discussed in Supplemental Results, we are able to recognize the loss of this site (Glazer et al., 2008).

Of the 22 structures selected for this work, 5 required slight alterations, as described in Supplemental Experimental Procedures (available online). All these were relatively modest, consisting of easily filled missing atoms or small gaps of missing residues or modified residues that could be easily replaced with the naturally occurring ones.

Molecular Dynamics Simulations

After the initial equilibration period, the energy analysis (data not shown) for each simulated system showed no significant change in potential energy over time and the root-mean-square deviation to the starting structure generally plateaued below 6 Å, suggesting that all systems were stable. In addition, the secondary structure content for each system simulated also showed no significant change over the course of the simulations (see Table 2). The trajectories were sampled every 2.5 ps and those

Table 2. Details of Simulation Systems and Analysis of MD Trajectories

Structures PDB ID	Chain Used	Ca^{2+} Present	Ions Other	Ions Added	% Initial Content	% Average Content	% Final Content
1B9A	Single	2		1 Na^+	50, 13	47, 12	44, 10
1B8C	A		1 Mg^{2+}	3 Na^+	50, 13	51, 10	56, 6
1K94	A	2		1 Cl^-	61	55	51
1F4Q	B			4 Na^+	62	53	52
3DNI	Single	2		5 Na^+	25, 26, 8	23, 24, 9	24, 25, 7
1DNK	A			9 Na^+	25, 26, 9	25, 23, 10	24, 27, 12
1I40	Single	5	1 Na^+, 3 Cl^-	None	17, 31, 17	20, 27, 10	23, 22, 9
1MJW	A		So_4^{2-}	8 Na^+	17, 33, 18	19, 28, 10	21, 24, 7
1K96	Single	2		1 Cl^-	71	61	47
1K8U	Single			3 Na^+	63	62	55
1PSH	A	1		1 Na^+	45, 14	40, 12	39, 7
1A3D	Single		1 Na^+	2 Na^+	45, 15	38, 16	43, 13
1NLS	Single	1	1 Mn^{2+}	5 Na^+	46, 12	41, 9	41, 8
1DQ0	Single			7 Na^+	46, 12	41, 8	38, 8
1F6S	F	1		5 Na^+	32, 15	27, 17	21, 19
1F6R	A			6 Na^+	31, 19	26, 17	26, 15
3LHM	Single	1		8 Cl^-	30, 27	28, 20	27, 21
2LHM	Single			6 Cl^-	30, 27	35, 19	33, 17
1QMD	A	3	2 Zn^{2+}	2 Na^+	40, 15, 10	35, 13, 11	29, 9, 13
1QM6	A		2 Zn^{2+}	9 Na^+	40, 15, 10	36, 14, 8	34, 15, 7
2POR	Single	3		28 Na^+	57, 12	49, 12	48, 8
3POR	Single			34 Na^+	57, 12	48, 14	50, 10

Column 1 lists PDB IDs of the structures used in this work. Column 2 shows which chain was used for the simulations. Column 3 lists how many calcium ions are present in the starting structure, which is also the number of calcium ions that were present in the system during simulation. Column 4 lists what other ions were originally present with the structure. Column 5 lists how many ions were added to each system in order to ensure neutral simulation conditions. The next three columns list the secondary structure (ss) content of the initial PDB structure, column 6, the average ss content over the course of the simulation, column 7, and the ss content of the final structure generated by the MD simulations, as calculated by the do_dssp program from the GROMACS suit. For the 1K94, 1F4Q, 1K96, and 1K8U only α-helical content is reported. For the 1B9A, 1B8C, 1PSH, 1A3D, 1F6S, 1F6R, 3LHM, and 2LHM, the two numbers in each column stand for α-helical and turn contents. For the 1NLS, 1DQ0, 2POR, and 3POR, the two numbers in each column stand for the β-sheet and turn contents. For the 1I40, 1MJW, 3DNI, 1DNK, 1QMD and 1QM6 the three numbers in each column stand for α-helical, β sheet and turn contents.

structures were evaluated by both FEATURE and the valence method (see Experimental Procedures). All simulation trajectories are available at https://simtk.org/home/mdfxnpredict.

Results of the HOLO-APO Pairs

FEATURE examines local 3D structural environments looking at ~80 features in six concentric spherical shells 1.25 Å apart (Halperin et al., 2008). Based on a model that is built by comparing true sites and nonsites for a given property, FEATURE then assigns a score to local environments, which describes how likely they are to represent one of interest. Coupling FEATURE to the structural dynamics of molecules considerably improved its performance, revealing 22 more Ca^{2+} binding sites in addition to the 15 (9 in the HOLO and 6 in the APO initial PDB structures) found readily by FEATURE alone. In addition to the true Ca^{2+} binding sites, FEATURE found 7 false-positive sites in the HOLO and 9 in the APO structural ensembles. A number of these are nonetheless interesting, as described below. The overall distributions of scores for static structures and for structures sampled during the molecular dynamics were not significantly different (see Figure 2). As expected, points that scored poorly for calcium binding were generally within the hydrophobic protein cores or at the structural periphery, where there were not enough atoms for the FEATURE algorithm to consider.

In order to test the generality of our approach to improve structure-based function prediction, we tested a second method that identifies Ca^{2+} binding sites in 3D environments. This method (Nayal and Di Cera, 1994) relies on measuring the negative charge around a potential site. Performance of the valence method also showed marked improvement with MD: it identified 15 Ca^{2+} binding sites in the HOLO structural ensembles, but only 3 in the initial HOLO structures.

Because FEATURE generally performed better than the valence method, the remainder of this section is focused on some results with FEATURE, which are presented below for selected HOLO-APO pairs. Results for the remaining pairs are presented in Supplemental Results, and Table 1 summarizes all results.

3DNI and 1DNK [Bovine DNase I]

The results of FEATURE scanning for the 3DNI-1DNK HOLO-APO pair were particularly interesting. This molecule contains only two Ca^{2+} binding sites, based on the simple scheme of

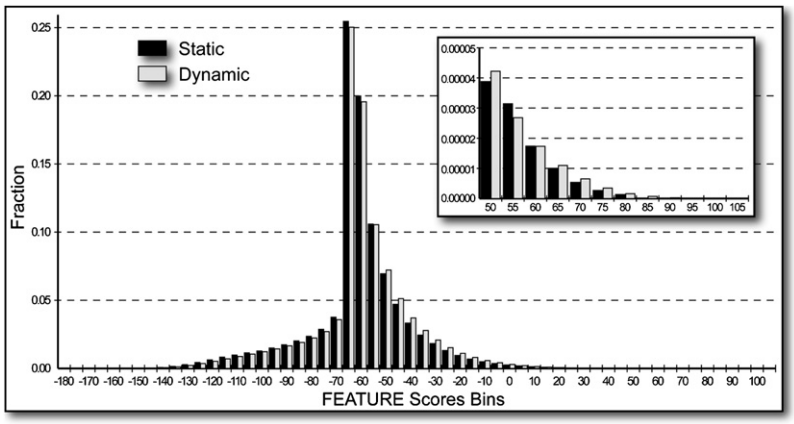

Figure 2. Global Grid Scanning Histogram
Global grid results for all 11 starting structures (black) and all 11 structural ensembles (light gray) are shown. The minimum and the maximum scores attained are ~−177 and ~105, respectively. The peak at ~−65 is formed by points that lie on the periphery of structures such that FEATURE evaluates the empty space around the structure. The inset illustrates the magnification of the right tails of the histograms for scores 50 and above.

relating our results to the Ca^{2+} ions bound within the HOLO structure (see Experimental Procedures). However, literature investigation revealed that this molecule contains one more characterized Ca^{2+} binding site at the active site (Suck et al., 1984). Although only revealing a single site in the HOLO and APO initial PDB structures, FEATURE correctly identified all three Ca^{2+} binding sites in the HOLO structural ensemble (see Figure 3A). In the APO structural ensemble, the Ca^{2+} binding site at the active site of the molecule and CA282 site were revealed.

*1I40 and 1MJW [*Escherichia coli *Inorganic Phosphatase]*

In the case of the HOLO structure 1I40, our results showed a dependence on the initial structure with which MD simulation was started. In the 1I40 starting structure, CA306 is an active site cation, which usually binds in the presence of the protein substrate. However, because the substrate is absent, this Ca^{2+} ion is not in its native position and is instead located 5.3Å away from the CA302 binding site, which influences the clustering analysis to lump the two sites into one (see Supplemental Experimental Procedures, section 2). The high-scoring putative Ca^{2+} binding site centers obtained with global grid FEATURE scanning spanned two different environments coordinated by different sets of amino acids, having in common only ASP157 (see Supplemental Movies). Because these environments correspond well to the two Ca^{2+} binding sites, CA302 and CA306, we conclude that our method locates both of those sites. The coordination environment of CA304 in this molecule consists of six water molecules and one oxygen atom from the protein itself. Because water molecules are not reliably present in crystal structures, FEATURE does not consider them in its models, and thus would be unlikely to recognize calcium sites coordinated mostly by water for either HOLO or APO structures. FEATURE does not identify any of the sites in the APO initial PDB structures or the APO structural ensemble.

1K96 and 1K8U [Human S100A6]

Although both of the expected Ca^{2+} binding sites present in the 1K96 HOLO structure were readily identified in the initial PDB structure and the structural ensemble, no Ca^{2+} binding sites were identified in its counterpart APO 1K8U system. However, the site noted as CA91 in the HOLO structure achieved scores close to the model threshold in the APO dynamic ensemble. In order to investigate whether a longer simulation might uncover this site, we continued the 1 ns simulation for an additional 9 ns. The longer trajectory contained 4001 structures sampled every 2.5 ps, of which several attained a FEATURE score of more than 50, compatible with Ca^{2+} binding at the CA91 site, especially around the eighth nanosecond.

1F6S and 1F6R [Bovine α-Lactalbumin] and 3LHM and 2LHM [Human Lysozyme]

On the sequence and structural levels lysozyme and α-lactalbumin exhibit very high similarity, and have been postulated to be evolutionarily related: emerging from a duplication of a single ancestral gene and then diverging in their functions over time

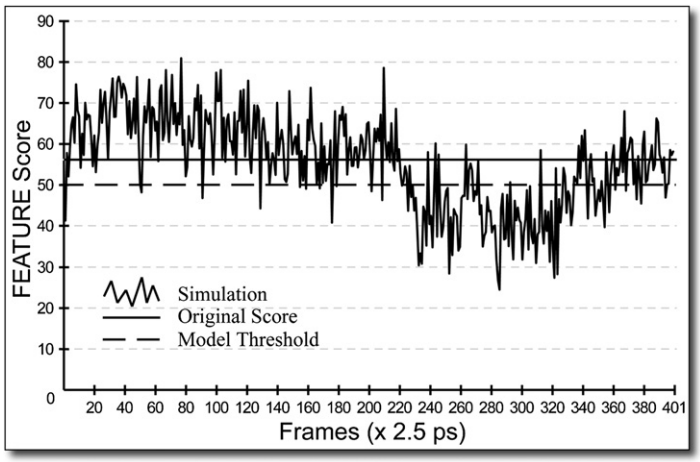

Figure 3. Local Grid FEATURE Scanning Results for a 1 ns Simulation of 1I40 around the CA302 Site
A trace of the local grid FEATURE scanning for CA302 Ca^{2+} binding site of the HOLO 1I40 structural ensemble is shown in solid black. The horizontal black line indicates the highest score obtained for this site on a local grid in the starting structure. The model threshold is represented by a dashed line. Over the course of the simulation, several structures reveal the presence of favorable Ca^{2+} binding environments, by obtaining scores of 50 or above. The short dip of scores under the threshold between 0.55 ns and 0.85 ns is well explained by a local rearrangement in one of the residues coordinating this binding site. The Supplemental Movies depict this change in the structure and further show how this particular residue settles toward the end of the simulation to accommodate this binding site and another one nearby.

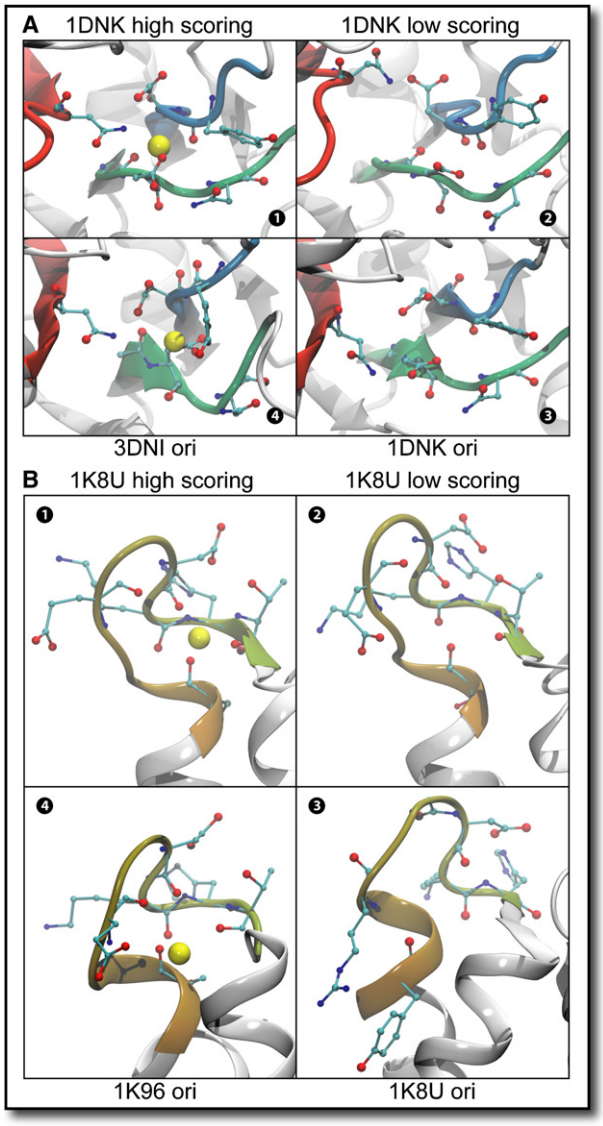

Figure 4. Close-up of Several Ca^{2+} Binding Sites

The side chains of nearby residues are shown, with cyan representing carbon, red oxygen, and blue nitrogen atoms. The backbone of these residues is also colored by index from red to blue. The yellow balls represent the putative site centers of the Ca^{2+} binding sites as identified by FEATURE, scoring over 50 on global grid FEATURE scanning.

(A) Close-up of the Ca^{2+} binding site located at the active site of the HOLO-APO pair 3DNI-1DNK The red, blue, and green strands illustrate that disparate parts of the molecule come together to form this binding site. 1. 1DNK highest scoring conformation is shown. 2. 1DNK low scoring conformation is shown. 3. 1DNK site as it appears in the original PDB file is shown. 4. 3DNI conformation is shown which scores similarly to the highest scoring 1DNK conformation.

(B) Close-up of the CA91 binding site in the HOLO-APO pair 1K96-1K8U and the 10 ns result of 1K8U. The single flexible loop illustrated in each panel defines this Ca^{2+} binding site. 1. 1K8U highest scoring conformation from the 10 ns MD simulation is shown. 2. 1K8U low scoring conformation is shown. 3. 1K8U site as it appears in the original PDB file is shown. 4. 1K96 conformation is shown that scores similarly to the highest scoring 1K8U conformation.

(Qasba and Kumar, 1997). As such, it is rather encouraging that FEATURE successfully identified the Ca^{2+} binding site present in these molecules in the HOLO and APO structural ensembles. Interesting, also, is the fact that an identical false-positive site was identified in all four structural ensembles. In the human lysozyme, residues THR52, SER61, ASP67, THR70, and others nearby persistently directed available oxygen atoms toward the false-positive site, and could also participate in the binding coordination of a divalent cation. The location of this false-positive site was far from the locations of zinc and manganese ions binding sites. The Ca^{2+} binding model employed by FEATURE for this work correctly did not detect these binding sites.

DISCUSSION

The purpose of these experiments was to test the hypothesis that short MD simulations can improve the performance of function recognition methods. Figure 3 depicts a trace of local grid FEATURE scanning around the CA302 binding site in the 1I40 HOLO structural ensemble. This particular site is easily recognized by FEATURE as a Ca^{2+} binding site without the help of MD simulations, evidenced by the highest score of ~56 attained by the initial PDB structure at this site. However, these results illustrate clearly that even HOLO crystal structures do not necessarily contain the more favorable local conformations for Ca^{2+} binding, whereas MD simulations have the potential to reveal structures that do: over the course of the simulation, many structures were generated that scored much higher than the initial structure. Nearly all the sites conformed to this trend. In addition, sites exhibited dynamic behavior: the side chains within the sites changed between coordinated and uncoordinated states. On average, in order for FEATURE to identify the sites in the structural ensembles that were not obvious in the starting structures, the side chains coordinating calcium binding moved by 3 Å (data not shown).

This work demonstrates the value of examining molecular motions in the course of predicting function. In general, FEATURE performed better on the initial HOLO structures than the valence method, and the MD simulations improved the results of both methods for the HOLO structural ensembles. FEATURE outperformed the valence method in predicting Ca^{2+} binding sites for both the APO starting structures and the MD-generated structural ensembles, which also showed marked improvement in FEATURE results. As expected, for both methods, Ca^{2+} sites in the APO structures were more challenging to recognize than the corresponding sites in the HOLO structures. The presence of the Ca^{2+} ion in the binding sites of the HOLO structures might influence the topology of the sites, with side chains adopting favorable conformations more often. In contrast, the APO side-chain conformations are not similarly constrained, and hence might form favorable Ca^{2+} binding states more transiently.

Both function prediction methods identified sites that were not documented to bind Ca^{2+} ions, which we label as false positive (FP). Most of these sites differed from the true Ca^{2+} binding sites in two ways. First, the highest score achieved in the true-positive (TP) clusters tended to be much higher than the highest score observed in the FP clusters. Also, FP clusters tended to consist of one or two putative site centers, whereas the TP clusters were mostly composed of multiple putative site centers (see

Table 3. Filtered Clustered Data

FEATURE Scores			Number of Hits in Cluster		
PDB ID	Site	Highest Score	PDB ID	Site	Number of Hits
1QMD	Zn site	111.24	1QMD	Zn site	24,467
1B8C	CA109	100.39	1QM6	Zn site	10,456
1QMD	CA405	100.19	3DNI	CA282	5,824
3DNI	CA282	95.56	1B8C	CA109	5,342
1QM6	Zn-site	94.08	1QMD	CA405	4,796
1F6S	CA124	87.67	1F6S	CA124	3,506
1I40	CA302	87.25	1NLS	CA239	2,172
1B9A	CA109	86.23	1I40	CA302	2,121
2POR	CA303	83.90	1K96	CA92	1,843
1K96	CA92	82.76	1QM6	CA405	1,437
1K94	CA998	82.11	2POR	CA303	1,215
1QM6	CA405	79.38	1K94	CA998	660
1NLS	CA239	72.57	1B9A	CA109	468
1QM6	***FP1***	71.63	1DQ0	CA239	223
3POR	CA304	71.02	3DNI	CA281	169
1F6S	***FP1***	70.00	1QM6	***FP1***	145
1F6R	CA124	69.02	1F6S	***FP1***	124
3DNI	CA281	65.41	1F6R	***FP1***	123
1I40	CA306	65.07	1F6R	CA124	97
1DQ0	CA239	64.99	3POR	CA304	85
1K94	***FP1***	64.08	2POR	CA304	75
1K96	CA91	64.06	1I40	CA306	61
2POR	CA304	63.88	1DNK	Active site	51
1F4Q	CA998	63.62	3POR	CA303	51

Table 3. *Continued*

FEATURE Scores			Number of Hits in Cluster		
PDB ID	Site	Highest Score	PDB ID	Site	Number of Hits
3POR	CA303	63.44	2LHM	***FP1***	50
1DNK	CA282	63.20	3LHM	***FP1***	46
1F6R	***FP1***	62.99	1A3D	CA120	36
1A3D	CA120	62.67	1DNK	CA282	34
2LHM	***FP1***	62.23	2POR	Ca4	29
1QMD	***FP1***	61.89	1K94	***FP1***	23
3LHM	***FP1***	61.24	3POR	***FP1***	22
3LHM	CA131	60.15	1QMD	***FP1***	18
2POR	***FP1***	60.05	2LHM	CA131	18
2LHM	CA131	59.94	1NLS	***FP1***	17
1QM6	***FP2***	59.34	1K96	CA91	15
3DNI	Active site	58.78	1K8U_8ns	CA92	15
1DNK	Active site	58.33	1F4Q	CA998	13
1NLS	***FP1***	57.76	3POR	CA302	13
2POR	Ca4	57.71	1QM6	***FP2***	10
3POR	***FP1***	57.31	2POR	***FP1***	10
3POR	***FP2***	56.44	3DNI	Active site	9
1QM6	***FP3***	56.41	3LHM	CA131	9
1K8U_8ns	CA92	56.38	3POR	Ca4	9
3POR	CA302	56.05	1QM6	***FP3***	7
3POR	Ca4	55.95	2POR	CA302	7
1PSH	***FP1***	55.59	1F4Q	***FP1***	6
2POR	CA302	55.04	3POR	***FP2***	5
1F4Q	***FP1***	54.32	1PSH	***FP1***	4
1QM6	***FP4***	53.68	1B9A	CA110	3
1B9A	CA110	50.62	1QM6	***FP4***	3

The table lists the filtered clustered data in two ways: sorted by the highest FEATURE score obtained within the cluster and by the number of the identified putative Ca^{2+} binding sites in each supercluster. Columns 1 and 4 show the PDB ID of the molecule in which the site is located. Columns 2 and 5 list either the Ca^{2+} binding sites that were identified or the name of the FP result. Column 3 lists the highest FEATURE score obtained by the specified cluster, and column 6 lists the number of the putative Ca^{2+} binding sites identified in each supercluster, starting with at least 3.

Table 3 and Figure 5). Based on positive predictive value analysis, we required that at least three putative site centers be present at the site for it to be counted as a TP or FP result. Only 16 FP results identified by FEATURE survived this filter, out of a possible 35 for FEATURE and 29 for the valence method, whereas only 2 and 10 TP results were lost for FEATURE and valence method, respectively. All the results reported in this work survived this filter. Examination of the trade-off between the number of obtained TP and FP sites is also possible through varying the score cut-offs for FEATURE and the valence method. Such future investigations might be worthwhile.

The accuracy of the force fields in treating Ca^{2+} interactions with the protein and solvent might be a limiting factor in our results. A recent study demonstrated that GROMOS force field underestimated by 2-fold the attractive interactions between the Ca^{2+} ions and protein side chains involved in binding coordination (Project et al., 2007). This same study implicated CHARMM and OPLS-AA force fields in underestimating by 2-fold and overestimating by 4-fold those same interactions. Improvements in force field parameters could further improve the efficiency of Ca^{2+} binding recognition when coupling structure-based function prediction methods to MD simulations. With better parameterization, it might be appealing to introduce Ca^{2+} atoms in the high-scoring APO sites in the MD protocol in order to see if these sites continue to exhibit the high-scoring conformations in the presence of the cation. In our experiments, several APO Ca^{2+} binding sites narrowly missed the threshold score of 50: 1DNK CA281, 1MJW CA302 and CA306, and 1K8U CA91 (1 ns simulation). It is possible that if Ca^{2+} were included in the APO systems in the MD simulations, the ions could enhance further the higher-scoring conformations.

Our results, especially for the APO structural ensembles, conform to the pre-existing equilibrium hypothesis of ligand-binding, where the molecule exists in an equilibrium of several different conformations. The binding of a ligand to the appropriate conformation shifts the equilibrium toward this particular conformation (Keskin, 2007; Tobi and Bahar, 2005; Tsai et al., 1999; Xu et al., 2008). Therefore, even without the presence of a calcium ion, the APO structures might exhibit transient conformations favorable for calcium binding. In fact, with the addition of Ca^{2+} atoms to the APO sites in the MD simulations protocol we would not expect qualitative differences in the results, other

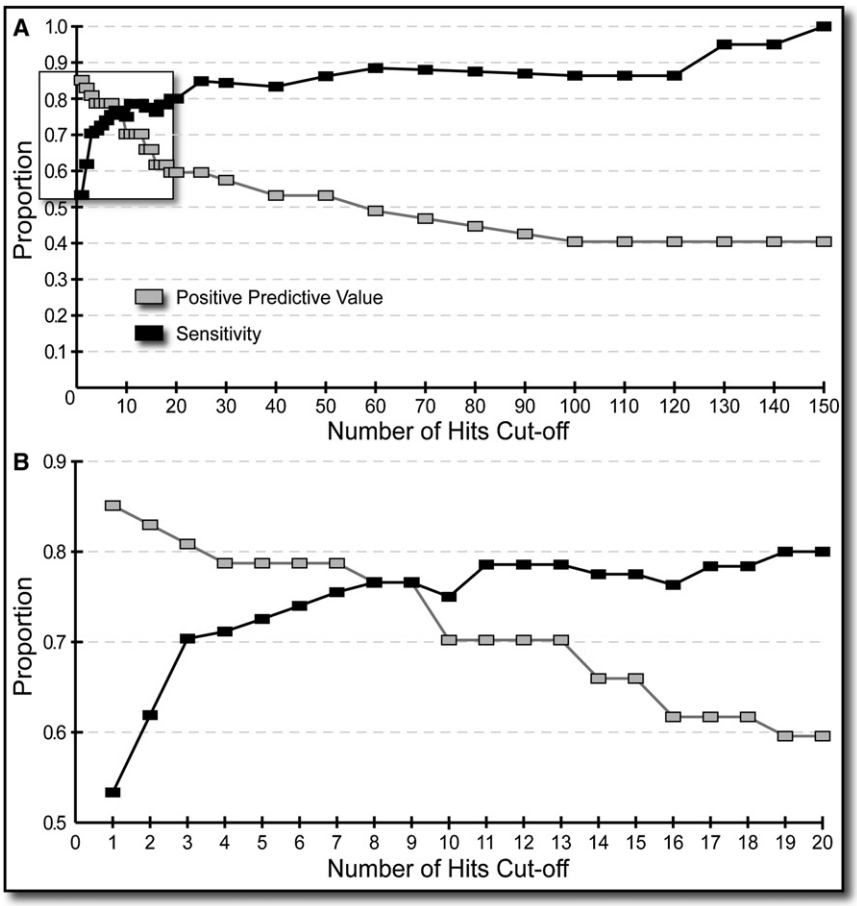

Figure 5. Analysis of Trade-off between TP and FP

The figure illustrates full analysis of our raw data with regards to the number of the identified putative Ca^{2+} binding site centers in each supercluster. (A) Positive predictive value and sensitivity with respect to the number of the identified putative Ca^{2+} binding site centers in each supercluster (see Table 3).

(B) Close-up of the first 20 data points in (A), outlined with the rectangle. From these plots, especially B, we chose to filter our raw clustering results with the condition that a valid supercluster must contain at least three putative Ca^{2+} binding site centers.

than perhaps an increase in the frequency and persistence of high-scoring conformations.

Currently, MD simulations remain a rather expensive way of generating structural diversity. The protocol used in this work relied on the simplicity of the function of interest. The 1 ns simulations generally proved to be long enough, generating sufficient number of conformations to elicit positive identification of the existing Ca^{2+} binding sites (it is important to remember that our goal was simply to generate representative conformations—it was not required that the conformations were sampled with a Boltzmann probability). Several improvements can be made to this protocol, including allowing longer times for system equilibration and trying different force fields. However, such steps would be impossible to predict if the work concerned a structure with an unknown function.

Our experiments are not sufficient to provide statistically significant estimates of the improved performance of structure recognition. However, for many structures, we observed (as described above and in Supplemental Results) conformational dynamics that contributed to the formation of calcium binding pockets. With improvements in MD algorithms and implementations on special purpose hardware, it might become possible to run the dynamics for a longer period and to apply the algorithm described here on a large scale to many proteins in the PDB (Friedrichs et al., 2009). This paper reveals the potential value of such an effort at uncovering otherwise obscure binding sites.

Conclusions

The dynamic ensembles generated by the MD simulations improved the performance of two different structure-based function prediction methods. Both function recognition algorithms achieved better performance in identifying Ca^{2+} binding sites in structural ensembles generated by the MD simulations in 1 ns, than in the initial structures obtained from the PDB. We expect that our methodology can be easily amended to accommodate large systems or those that require significant domain motions for function determination by either generating longer simulations or employing other methods that explore conformational space more rapidly, such as normal modes or replica exchange. Furthermore, although this work employed FEATURE and the valence method, which are simple and efficient to apply in a large-scale study to hundreds and thousands of structures, it should be apparent from our results that any other structure annotation algorithm can be accommodated by the methodology outlined in this work. As such, the scheme for recognizing function based on structures summarized in Figure 1 should be applicable to the novel unannotated structures generated by the Structural Genomics Consortia.

EXPERIMENTAL PROCEDURES

Structures and Definition of the HOLO and APO Sets of Ca^{2+} Binding Sites

The following structures were taken from the PDB for this work: carp parvalbumin β, 1B9A (Cates et al., 1999) and 1B8C (Cates et al., 1999), human grancalcin, 1K94 (Jia et al., 2001) and 1F4Q (Han et al., 2000), bovine DNase I, 3DNI (Oefner and Suck, 1986) and 1DNK (Weston et al., 1992), *Escherichia coli* inorganic phosphatase, 1I40 (Samygina et al., 2001) and 1MJW (Avaeva et al., 1998), human S100A6, 1K96 (Otterbein et al., 2002) and 1K8U (Otterbein et al., 2002), *Naja naja naja* phospholipase A_2, 1PSH (Fremont et al., 1993) and 1A3D (Segelke et al., 1998), *Canavalia ensiformis* concanavalin A, 1NLS (Deacon et al., 1997) and 1DQ0 (Bouckaert et al., 2000), bovine α-lactalbumin, 1F6S and 1F6R (Chrysina et al., 2000), human lysozyme, 3LHM and 2LHM (Inaka et al., 1991), *Clostridium perfringens* alpha-toxin, 1QMD and 1QM6 (Naylor et al., 1999), and *Rhodobacter capsulatus* porin, 2POR (Weiss and Schulz, 1992) and 3POR (Weiss and Schulz, 1993).

The 24 Ca^{2+} binding sites that formed the HOLO set were defined as the sites in which Ca^{2+} ion was present in the original static structures of 1B9A, 1K94, 3DNI, 1I40, 1K96, 1PSH, 1NLS, 1F6S, 3LHM, 1QMD, and 2POR with five exceptions. Only CA302, CA304, and CA304 sites were used for the 1I40 case. The active site of 3DNI and the fourth Ca^{2+} binding site of 2POR are characterized Ca^{2+} binding sites (Suck et al., 1984; Weiss and Schulz, 1992), and although no Ca^{2+} is present at these sites in the original PDB structures, we included them in our data set. Similarly, the zinc binding site of 1QMD was included as an expected site (see Supplemental Results). As such, there were 21 occupied and 3 unoccupied Ca^{2+} binding sites in the HOLO data set.

By definition, the APO structures do not contain Ca^{2+} ions. However, because these APO structures directly correspond to the HOLO structures, we expected to observe the Ca^{2+} binding sites in analogous positions. With the exception of the CA110 binding site of 1B8C, discussed above, 23 of the 24 sites forming the HOLO data set are also present in the APO structures, which consisted of 1B8C, 1F4Q, 1DNK, 1MJW, 1K8U, 1A3D, 1DQ0, 1F6R, 2LHM, 1QM6, and 3POR.

Supplemental Experimental Procedures section 1 describes minor modifications made to some of the structures in order to ensure system completeness during the MD simulations.

Molecular Dynamics Simulations

GROMACS is a software suite that allows generation and analysis of MD simulations (Lindahl et al., 2001). Using GROMACS version 3.3.1, we created 1 ns simulations of the 11 pairs of structures in order to generate structural diversity for each protein set. For each of the structures, the system consisted of only one chain and appropriate ions, a 1 nm layer of solvent, simple point charge (Berendsen et al., 1981) water molecules, and sodium or chloride ions for neutralization (see Table 2).

Each system, treated with a periodic boundary condition, underwent a 200-step energy minimization using the steepest descent algorithm followed by a 10 ps harmonic position restrained MD simulation at 300 K, in which all the protein atoms remained motionless. Electrostatic and Van der Waals interactions and neighborlist cut-offs were set at 1 nm. Separate external temperature baths (Berendsen et al., 1984) of 300 K and coupling constant tau_T = 0.1 ps were used for the protein and nonprotein components of each system. The 1 ns production run simulation was carried out at constant pressure of 1 bar, kept as such by coupling weakly to pressure baths (Berendsen et al., 1984) with tau_P = 0.5 ps, and constant temperature, as above. An integration time step of 2 fs was used with the LINCS (Hess et al., 1997) algorithm, constraining all covalent bonds to their equilibrium lengths. The force field used was GROMOS96 (van Gunsteren et al., 1996), 43a1. Generation of these trajectories took between 12 to 36 hr on a single 2.8 GHz processor with 2 G RAM. For each system, a structural ensemble was created by extracting structures generated by the simulation every 2.5 ps.

FEATURE Scanning

This work employed FEATURE version 1.9 (Wei and Altman, 2003) and the Ca^{2+} binding site model built by Wei and Altman (1998) for analysis of static starting structures and structural ensembles generated by the MD simulations. A score of 50 or above at a given point in the structural space identified a putative Ca^{2+} binding site center.

FEATURE scanning was implemented in two ways: global grid and local grid. A global grid of points 1 Å apart was created to encompass each starting structure and those generated by simulations. At each point, FEATURE algorithm calculated a score using the Ca^{2+} binding site model. For each structure examined, coordinates of the points which scored at least 50 were retained for clustering analysis described below. When looking at a novel structure, the global grid scanning would be applied as an initial analysis. Putative sites identified by the global grid scanning could then be followed up with the local grid scanning analysis, which allows examination of the behavior of the site of interest in finer detail. In our case, we were only interested in the true Ca^{2+} binding sites. Therefore, a local 10 × 10 × 10 $Å^3$ grid of points 1 Å apart was created to encompass the Ca^{2+} binding sites of each starting structure and those generated by simulations. For each HOLO-APO pair, the local grids were centered on an equivalent atom, which was identified to be the closest to the Ca^{2+} atom in the crystallized HOLO structure. FEATURE algorithm calculated a score at each point using the Ca^{2+} binding site model. For each structure examined, only the information about the highest-scoring point was retained for visualizing behavior of the sites over the course of the simulations (see Figure 4).

Figure 2 illustrates the distributions of all the scores at the global grid points within 7.5 Å of at least one atom in the structures, which is the radius of the FEATURE Ca^{2+} binding model, for the starting PDB structures and the respective structural ensembles generated by the MD simulations. We compared the two distributions using the chi-square goodness-of-fit test: the distribution from the starting structures was considered as theoretical values and the distribution from the structural ensembles was considered as the observed values. This analysis required counts for the calculations, so we normalized the structural ensembles distribution to the number of structures examined in each structural ensemble by reducing the number of counts for each bin by a factor of 401. The two distributions are statistically the same (calculations not shown).

As a negative control, we scanned with local grid areas that were not near the Ca^{2+} binding sites in 1B9A, 1K94, and 1K96 HOLO structural ensembles. In each case, an atom was selected to be the grid center by two criteria: the atom density surrounding this atom in a sphere of radius 7.5 Å and its distance to the surface were comparable to those of the central atoms of the local grids at the true Ca^{2+} binding sites. The local environments surrounding these points never attained conformations suitable for Ca^{2+} binding; the highest FEATURE scores never exceeded 30, and had a mean value of −10 for all frames in the simulations tested (data not shown). These results demonstrate that the score threshold of 50 established using static structures is a reasonably stringent cut-off to be applied to FEATURE scanning of structural ensembles generated by the MD simulations.

Valence Scanning

We used the valence method (Nayal and Di Cera, 1994) with default parameters to scan the starting structures and the ensembles generated by the MD simulations. Valence is the number of electrons shared by an ion during bond-formation, and is generally estimated as the overall charge of the ion (thus, Ca^{2+} has valence of 2). This method further assumes that atoms exert partial valence at a distance, which decreases as the distance from the ion increases. Thus, in order to locate putative ion binding sites, this method sums partial valencies provided by nearby atoms. In our tests, a point around which partial valencies summed to 1.4 or above was used for predicting Ca^{2+} binding. A step size of 1 Å was chosen to allow comparison between valence method and FEATURE results.

Clustering Algorithm to Define True- and False-Positive Results

Both function-recognition methods applied in this study might identify multiple putative Ca^{2+} binding site centers in a local region that often represent the same site. Additionally, combining and analyzing global scanning results of FEATURE and the valence method posed a challenge, because the gold standard Ca^{2+} binding sites (defined by the HOLO structures) are difficult to define once the molecules start moving during the simulations. In general, it is challenging to compare sites in different structures, because they are separated by time and conformational motion. Accordingly, we devised a clustering algorithm that considers the nearest 50 atoms to a point, such as a known Ca^{2+} site, and uses a paired Wilcoxon rank sum test to assess the similarity of two points in two potentially very different structural conformations. The nearest 50 atoms were chosen because they typically filled a sphere of the volume used in scanning by FEATURE (radius = 7.5 Å).The putative site centers identified by FEATURE or the valence method were clustered in order to define predicted Ca^{2+} binding sites that were substantially the same across the MD trajectories. All results reported and discussed in this manuscript are based on this clustering analysis (see details in Supplemental Experimental Procedures section 2) and a post-clustering filter (see Discussion).

Structure and Trajectory Visualization

We used Visual Molecular Dynamics (VMD) (Humphrey et al., 1996) in order to visualize structures and trajectories generated by the MD simulations, as well as the results of FEATURE and the valence method scanning. Images of structures were generated using Tachyon Ray Tracer (Frishman and Argos, 1995; Stone, 1998) from within the VMD.

SUPPLEMENTAL DATA

Supplemental Data include two movies, Supplemental Experimental Procedures, and Supplemental Results and can be found with this article online at http://www.cell.com/structure/supplemental/S0969-2126(09)00222-6.

ACKNOWLEDGMENTS

This work is supported by NIH LM-05652 and the SIMBIOS National Center for Simulation of Biological Structures, GM-072970. D.S.G. is also supported by the Stanford Genome Training Grant NIH 5 T32 HG00044. We thank Inbal Halperin, members of the Stanford Helix group, and the SIMBIOS National Center for useful discussions.

Received: October 15, 2008
Revised: May 6, 2009
Accepted: May 6, 2009
Published: July 14, 2009

REFERENCES

Avaeva, S.M., Rodina, E.V., Vorobyeva, N.N., Kurilova, S.A., Bazarova, T.I., Sklyankina, V.A., Oganessyan, V.Y., Samygina, V.R., and Harutyunyan, E.H. (1998). Three-dimensional structures of mutant forms of *E. coli* inorganic pyrophosphatase with Asp->Asn single substitution in positions 42, 65, 70, and 97. Biochemistry (Mosc.) *63*, 671–684.

Berendsen, H.J.C., Postma, J.P.M., van Gunsteren, W.F., and Hermans, J. (1981). Interaction model for water in relation to protein hydration. In Intermolecular Forces, B. Pullman, ed. (Dordrecht, The Netherlands: D. Reidel Publishing Company), pp. 331–342.

Berendsen, H.J.C., Postma, J.P.M., van Gunsteren, W.F., Nola, A.D., and Haak, J.R. (1984). Molecular dynamics with coupling to an external bath. J. Chem. Phys. *81*, 3684–3690.

Berman, H.M., Westbrook, J., Feng, Z., Gilliland, G., Bhat, T., Weissig, H., Shindyalov, I., and Bourne, P. (2000). The Protein Data Bank. Nucleic Acids Res. *28*, 235–242.

Bouckaert, J., Dewallef, Y., Poortmans, F., Wyns, L., and Loris, R. (2000). The structural features of concanavalin A governing non-proline peptide isomerization. J. Biol. Chem. *275*, 19778–19787.

Cates, M.S., Barry, M.B., Ho, E.L., Li, Q., Potter, J.D., and Phillips, G.N., Jr. (1999). Metal-ion affinity and specificity in EF-hand proteins: coordination geometry and domain plasticity in parvalbumin. Structure *7*, 1269–1278.

Chandonia, J.M., and Brenner, S.E. (2006). The impact of structural genomics: expectations and outcomes. Science *311*, 347–351.

Chrysina, E.D., Brew, K., and Acharya, K.R. (2000). Crystal structures of Apo- and Holo-bovine α-Lactalbumin at 2.2-angstrom resolution reveal an effect of calcium on inter-lobe interactions. J. Biol. Chem. *275*, 37021–37029.

Damm, K.L., and Carlson, H.A. (2007). Exploring experimental sources of multiple protein conformations in structure-based drug design. J. Am. Chem. Soc. *129*, 8225–8235.

Deacon, A., Gleichmann, T., Kalb, A.J., Price, H., Raftery, J., Bradbrook, G., Yariv, J., and Helliwell, J.R. (1997). The structure of concanavalin A and its bound solvent determined with small-molecule accuracy at 0.94-angstrom resolution. J. Chem. Soc. Faraday Trans. *93*, 4305–4312.

Eyrisch, S., and Helms, V. (2007). Transient pockets on protein surfaces involved in protein - protein interaction. J. Med. Chem. *50*, 3457–3464.

Fetrow, J.S., Godzik, A., and Skolnick, J. (1998). Function analysis of the *Escherichia coli* genome using the sequence-to-structure-to-function paradigm: identification of proteins exhibiting the glutaredoxin/thioredoxin disulfide oxidoreductase activity. J. Mol. Biol. *282*, 703–711.

Frembgen-Kesner, T., and Elcock, A.H. (2006). Computational sampling of a cryptic drug binding site in a protein receptor: explicit solvent molecular dynamics and inhibitor docking to p38 MAP kinase. J. Mol. Biol. *359*, 202–214.

Fremont, D.H., Anderson, D.H., Wilson, I.A., Dennis, E.A., and Xuong, N.H. (1993). Crystal structure of phospholipase A_2 from Indian cobra reveals a trimeric association. Proc. Natl. Acad. Sci. USA *90*, 342–346.

Friedberg, I. (2006). Automated protein function prediction—the genomic challenge. Brief. Bioinform. *7*, 225–242.

Friedrichs, S., Eastman, P., Vaidyanathan, V., Houston, M., LeGrand, S., Beberg, A.L., Ensign, D.L., Bruns, C.M., and Pande, V.S. (2009). Accelerating molecular dynamic simulation on graphics processing units. J. Comput. Chem. *30*, 864–872.

Frishman, D., and Argos, P. (1995). Knowledge-based secondary structure assignment. Proteins *23*, 566–579.

Glazer, D.S., Radmer, R.J., and Altman, R.B. (2008). Combining molecular dynamics and machine learning to improve protein function prediction. Pac. Symp. Biocomput., 332–343.

Halperin, I., Glazer, D.S., Wu, S., and Altman, R.B. (2008). The FEATURE framework for protein function annotation: modelling new functions, improving performance, and extending to novel applications. BMC Genomics *16* (*Suppl 2*), S2.

Han, Q., Jia, J., Li, Y., Lollike, K., and Cygler, M. (2000). Crystallization and preliminary X-ray analysis of human Grancalcin, a novel cytosolic Ca^{2+}-binding protien present in leukocytes. Acta Crystallogr. D Biol. Crystallogr. *56*, 772–774.

Henzler-Wildman, K., and Kern, D. (2007). Dynamic personalities of proteins. Nature *450*, 964–972.

Hess, B., Bekker, H., Berendsen, H.J.C., and Fraaije, J.G. (1997). LINCS: a linear constraint solver for molecular simulations. J. Comput. Chem. *18*, 1463–1472.

Huang, S.Y., and Zou, X. (2007). Efficient molecular docking of NMR structure: application to HIV-1 protease. Protein Sci. *16*, 43–51.

Humphrey, W., Dalke, A., and Schulten, K. (1996). VMD - Visual Molecular Dynamics. J. Mol. Graph. *14*, 33–38.

Inaka, K., Kuroki, R., Kikuchi, M., and Matsushima, M. (1991). Crystal structures of the Apo- and Holomutant human lysozymes with an introduced Ca^{2+} binding site. J. Biol. Chem. *266*, 20666–20671.

Jia, J., Borregaard, N., Lollike, K., and Cygler, M. (2001). Structure of Ca^{2+}-loaded human Grancalcin. Acta Crystallogr. D Biol. Crystallogr. *57*, 1843–1849.

Karplus, M., and Kuriyan, J. (2005). Molecular dynamics and protein function. Proc. Natl. Acad. Sci. USA *102*, 6679–6685.

Karplus, M., and McCammon, J.A. (2002). Molecular dynamics simulations of biomolecules. Nat. Struct. Biol. *9*, 646–652.

Keskin, O. (2007). Binding induced conformational changes of proteins correlate with their intrinsic fluctuations: a case study of antibodies. BMC Struct. Biol. *7*, 31.

Levitt, M. (2007). Growth of novel protein structural data. Proc. Natl. Acad. Sci. USA *104*, 3183–3188.

Lindahl, E., Hess, B., and van der Spoel, D. (2001). GROMACS 3.0: a package for molecular simulation and trajectory analysis. J. Mol. Model. *7*, 306–317.

Meagher, K.L., and Carlson, H.A. (2004). Incorporating protein flexibility in structure-based drug discovery: using HIV-1 protease as a test case. J. Am. Chem. Soc. *126*, 13276–13281.

Nayal, M., and Di Cera, E. (1994). Predicting Ca^{2+}-binding sties in proteins. Proc. Natl. Acad. Sci. USA *91*, 817–821.

Naylor, C.E., Jepson, M., Crane, D.T., Titball, R.W., Miller, J., Basak, A.K., and Bolgiano, B. (1999). Characterisation of the calcium-binding C-terminal domain of *Clostridium perfringens* alpha-toxin. J. Mol. Biol. *294*, 757–770.

Oefner, C., and Suck, D. (1986). Crystallographic refinement and structure of DNase I at 2-angstrom resolution. J. Mol. Biol. *192*, 605–632.

Otterbein, L.R., Kordowska, J., Witte-Hoffmann, C., Wang, C.L., and Dominguez, R. (2002). Crystal structures of S100A6 in the Ca^{2+}-free and Ca^{2+}-bound states: the calcium sensor mechanism of S100 proteins revealed at atomic resolution. Structure *10*, 557–567.

Project, E., Nachliel, E., and Gutman, M. (2007). Parameterization of Ca^{2+}-protein interactions for molecular dynamics simulations. J. Comput. Chem. *29*, 1163–1169.

Qasba, P.K., and Kumar, S. (1997). Molecular divergence of lysozymes and alpha-lactalbumin. Crit. Rev. Biochem. Mol. Biol. *32*, 255–306.

Samygina, V.R., Popov, A.N., Rodina, E.V., Vorobyeva, N.N., Lamzin, V.S., Polyakov, K.M., Kurilova, S.A., Nazarova, T.I., and Avaeva, S.M. (2001). The structures of *Escherichia coli* Inorganic Pyrophosphatase complexed with Ca^{2+} or $CaPP_i$, at atomic resolution and their mechanistic implications. J. Mol. Biol. *314*, 633–645.

Segelke, B.W., Nguyen, D., Chee, R., Xuong, N.H., and Dennis, E.A. (1998). Structures of two novel crystal forms of *Naja naja naja* phospholipase A_2 lacking Ca^{2+} reveal trimeric packing. J. Mol. Biol. *279*, 223–232.

Sivanesan, D., Rajnarayanan, R.V., Doherty, J., and Pattabiraman, N. (2005). In-silico screening using flexible ligand binding pockets: a molecular dynamics-based approach. J. Comput. Aided Mol. Des. *19*, 213–228.

Stone, J. (1998). An efficient library for parallel ray tracing and animation. Masters' thesis, Computer Science Department, University of Missouri at Rolla, Rolla, Missouri.

Suck, D., Oefner, C., and Kabsch, W. (1984). Three-dimensional structure of bovine Pancreatic DNase I at 2.5 A resolution. EMBO J. *3*, 2423–2430.

Terwilliger, T.C. (2004). Structures and technology for biologists. Nat. Struct. Mol. Biol. *11*, 296–297.

Tobi, D., and Bahar, I. (2005). Structural changes involved in protein binding correlate with intrinsic motions of proteins in the unbound state. Proc. Natl. Acad. Sci. USA *102*, 18908–18913.

Tsai, C.J., Kumar, S., Ma, B., and Nussinov, R. (1999). Folding funnels, binding funnels, and protein function. Protein Sci. *8*, 1181–1190.

van Gunsteren, W.F., Billeter, S.R., Eising, A.A., Hünenberger, P.H., Krüger, P., Mark, A.E., Scott, W.R.P., and Tironi, I.G. (1996). Biomolecular Simulation: The GROMOS96 manual and user guide (Zürich, Switzerland: Hochschulverlag AG an der ETH Zürich).

Wallace, A.C., Borkakoti, N., and Thornton, J.M. (1997). TESS: a geometric hashing algorithm for deriving 3D coordinate templates for searching structural databases. Application to enzyme active sites. Protein Sci. *6*, 2308–2323.

Watson, J.D., Laskowski, R.A., and Thornton, J.M. (2005). Predicting protein function from sequence and structural data. Curr. Opin. Struct. Biol. *15*, 275–284.

Wei, L., and Altman, R.B. (1998). Recognizing protein binding sites using statistical descritions of their 3D environments (Maui, HI: In Pac. Symp. Biocomput), pp. 497–508.

Wei, L., and Altman, R.B. (2003). Recognizing complex, asymmetric functional sites in protein structures using a Bayesian scoring function. J. Bioinform. Comput. Biol. *1*, 119–137.

Weiss, M.S., and Schulz, G.E. (1992). Structure of porin refined at 1.8 angstrom resolution. J. Mol. Biol. *227*, 493–509.

Weiss, M.S., and Schulz, G.E. (1993). Porin conformation in the absence of calcium. J. Mol. Biol. *231*, 817–824.

Weston, S.A., Lahm, A., and Suck, D. (1992). X-ray structure of the DNase I-d$(GGTATACC)_2$ complex at 2-3-angstrom resolution. J. Mol. Biol. *226*, 1237–1256.

Wilson, C.A., Kreychman, J., and Gerstein, M. (2000). Assessing annotation transfer for genomics: quantifying the relations between protein sequence, structure and function through traditional and probabilistic scores. J. Mol. Biol. *297*, 233–249.

Wong, C.F., Kua, J., Zhang, Y., Straatsma, T.P., and McCammon, J.A. (2005). Molecular docking of balanol to dynamics snapshots of Protein Kinase A. Proteins *61*, 850–858.

Xu, Y., Colletier, J.P., Jiang, H., Silman, I., Sussman, J.L., and Weik, M. (2008). Induced-fit or preexisting equilibrium dynamics? Lessons from protein crystallography and MD simulations on acetylcholinesterase and implications for structure-based drug design. Protein Sci. *17*, 601–605.